High power microwave source for a plasma wakefield experiment

G. Shafir,[1] A. Shlapakovski,[1] M. Siman-Tov,[1] Yu. Bliokh,[1] J. G. Leopold,[1] S. Gleizer,[1] R. Gad,[1] V. V. Rostov,[2] and Ya. E. Krasik[1]
[1]*Physics Department, Technion, Haifa 36000, Israel*
[2]*Institute of High Current Electronics, Russian Academy of Sciences, Tomsk, Russia*

(Received 1 October 2016; accepted 24 December 2016; published online 17 January 2017)

The results of the generation of a high-power microwave (~550 MW, 0.5 ns, ~9.6 GHz) beam and feasibility of wakefield-excitation with this beam in under-dense plasma are presented. The microwave beam is generated by a backward wave oscillator (BWO) operating in the superradiance regime. The BWO is driven by a high-current electron beam (~250 keV, ~1.5 kA, ~5 ns) propagating through a slow-wave structure in a guiding magnetic field of 2.5 T. The microwave beam is focused at the desired location by a dielectric lens. Experimentally obtained parameters of the microwave beam at its waist are used for numerical simulations, the results of which demonstrate the formation of a bubble in the plasma that has almost 100% electron density modulation and longitudinal and transverse electric fields of several kV/cm. *Published by AIP Publishing.*
[http://dx.doi.org/10.1063/1.4973734]

I. INTRODUCTION

The research on laser-produced wakefields in plasma is of great interest because of the excitation of extremely high electric fields, which can be used for charged particle acceleration.[1–3] In the laser-wakefield accelerator, a laser pulse with intensity $I_0 > 10^{16}\,\mathrm{W/cm^2}$ and duration $\tau \approx 30\,\mathrm{fs}$ is focused into plasma with electron density $n_e \approx 10^{18}\,\mathrm{cm^{-3}}$. Because of the ponderomotive force generated by the strong gradient of the electric field of the pulse, a large electron density gradient is formed in the plasma. This results in high longitudinal electric fields, which can trap and accelerate a bunch of trailing electrons. The acceleration of electrons of a few GeV in the wakefield having an accelerating gradient $>100\,\mathrm{GV/m}$ has been demonstrated.[4] The plasma density modulation in laser-driven experiments is characterized by the time and length scales of ~50 fs and ~10 μm, respectively, which renders the direct diagnostics of the wakefield highly sophisticated. Therefore, most diagnostic methods are focused on the accelerated particles[5,6] or the application of the driving laser for plasma diagnostics.[7,8]

Wakefield excitation can be studied by applying an ultrashort high power microwave (HPM) pulse interacting with the plasma. Let us consider a microwave pulse with wavelength and duration of $\lambda = 3\,\mathrm{cm}$ and $\tau \approx 0.5\,\mathrm{ns}$, respectively, propagating in plasma having under-critical electron density $n_e \approx 10^{10}\,\mathrm{cm^{-3}}$. This pulse expels electrons from its path, by the ponderomotive force[9] $F_p = -(e^2/4m\omega^2)\nabla(E_{mw}{}^2)$, where e is the electron charge, m is the electron mass, ω is the microwave circular frequency, and E_{mw} is the amplitude of the microwave electric field. Considering a Gaussian profile of the cylindrical microwave beam, i.e., $E_{mw} = E_0 \exp(-r^2/\rho_0^2)$, which is tightly focused, $\rho_0 \approx 2\,\mathrm{cm}$, and equality between the ponderomotive force and the non-compensated space charge force formed by the plasma ions $F_{sc} = -eE_{sc}$, one can estimate the density modulation. Here let us note that for the microwave pulse with parameters listed above, the ponderomotive force of tightly focused microwave beam is directed mainly radially, as the pulse length is large as compared with the beam radius. Thus, the electric field, caused by radial separation of the plasma electrons and ions, can be estimated as $E_{sc} = 0.5e(\delta n)r/\varepsilon_0$ and the estimated density modulation $\delta n/n_0$ is as follows:

$$\frac{\delta n}{n_0} = 2\left(\frac{eE_{mw}}{\rho_0 m\omega\omega_p}\right)^2, \tag{1}$$

where n_0 is the density of non-disturbed plasma, $\omega_p = (n_0e^2/\varepsilon_0 m)^{1/2}$ is the plasma electron frequency, and ρ_0 is the spot radius of the microwave beam. With these parameters, one obtains a significant density modulation $(\delta n/n_0 > 0.2)$ at a microwave electric field amplitude $E_{mw} > 14\,\mathrm{MV/m}$. This electric field can be realized in microwave pulse with power $P > 160\,\mathrm{MW}$. The expected cycle duration of the plasma density modulation is ~1 ns with a typical length scale of ~10 cm allowing time- and space-resolved research of this phenomenon.

In earlier studies, the generation of plasma waves using microwaves was experimentally investigated with relatively low microwave power $(3 - 250\,\mathrm{kW})$ and long $(0.05 - 3\,\mu\mathrm{s})$ duration pulses.[10–13] In these studies, the effects of the microwave absorption, plasma density perturbation, microwave guiding, and ponderomotive force were investigated in both over- and under-dense plasmas. Also, in Ref. 14, the results of measurements of the plasma potential and bremsstrahlung radiation of electrons (energy $\leq$25 keV) accelerated by electric fields of plasma waves excited in plasma which is generated by microwave beam with power $\leq 100\,\mathrm{MW}$ (power density $\leq 10\,\mathrm{MW/cm^2}$, pulse duration of 50 ns) was reported. Analytical and numerical studies of the high-power and short duration microwave beam interaction with under-dense plasma in a rectangular waveguide resulting in the formation of wakefield and electron acceleration were also conducted.[15–17] However, the generation of plasma waves in preliminary formed under-dense plasma by a short duration (<1 ns) and extremely powerful microwave pulse ($>10\,\mathrm{MW/cm^2}$) with

strong radial and axial gradients of the electric field amplitude was not studied experimentally.

There are a number of different HPM sources capable of producing peak power up to several GW with duration <100 ns.[18] However, for the microwave energy of tens and hundreds J, high voltage drivers with large sizes (>10 m) and mass are required. For the case of microwave pulse duration ≤ 1 ns, the most suitable and compact HPM source for the research of wakefield generation is a superradiance backward wave oscillator (SR-BWO), which can generate from hundreds of MW to a few GW of peak power.[19–23] The most important difference between the SR-BWO and the long-pulse relativistic BWO is an extended length of the slow-wave structure (SWS). The coherence of the emission into a short single pulse is caused by self-bunching of the electron beam, which interacts with a slow spatial harmonic of the electromagnetic wave. The latter propagates along the electron beam with a group velocity having opposite direction with respect to the electron velocity. For X-band SR-BWO, the e-beam should be transported in a strong (>2.5 T) guiding magnetic field and the rise time of the current should be ≤ 1 ns. The optimal electron beam duration is equal to the sum of the electron propagation time in the BWO's SWS and the wave travelling time. For such conditions, a single pulse with a duration much less than that of the electron beam and peak power exceeding the electron beam power can be generated.[21,22] Using this approach, microwave pulses with central frequency, $f \approx 9.3$ GHz, peak power $P \approx 3$ GW, and full width half maximum (FWHM) duration $\tau_{mw} \approx 650$ ps were obtained.[23]

In this paper, we describe the development of a SR-BWO microwave source, generating a 9.6 GHz Gaussian microwave beam, with a peak power up to $\sim$550 MW and a duration (FWHM) of $\sim$0.5 ns. The microwave beam is focused using a dielectric lens onto a spot radius of $\sim$2 cm, where the interaction of the beam with plasma will be investigated. In addition, the results of preliminary numerical simulations for plasma-microwave interaction experiments are presented.

II. EXPERIMENTAL SETUP

The experimental system designed to investigate the HPM-plasma interaction, is shown in Fig. 1. The BWO is driven by a high-current relativistic electron beam generated in a magnetically insulated foilless diode under the application of a negative polarity high-voltage (HV) pulse, produced by a semiconductor-opening-switches (SOSs)-based generator[24] with an internal impedance of 200 Ω. The parameters of the diode and the generated electron beam were described previously,[25] where a generator producing HV pulses at a matched load of $\sim$220 kV, $\sim$6 ns at FWHM, and 1.5 ns rise-time was used. In order to increase the electron beam energy, the SOS-based generator was modified, resulting in the HV pulses of $\sim$350 kV, $\sim$6 ns at FWHM, and $\sim$0.5 ns rise-time obtained after the gas spark-gap switch at the matched (200 Ω) load. This modified generator allows an increase in electron energy up to $\sim$250 keV with a beam current amplitude of $\sim$1.5 kA. The modified generator can operate at a repetition rate of up to 1 kHz but the present experiments were carried out in a single-shot mode because of the limitations related to the magnetic field system.

The gas spark switch, placed at the output of the generator, was connected to the cathode holder. The length of the cathode holder and HV insulator interface was minimized to decrease the inductive voltage drop and the stray capacitance of the holder. An explosive emission plasma, formed at the sharp boundary of the edged graphite cathode (diameter of 28 mm) under the application of an HV pulse, served as a source of electrons that produced a $\approx$0.5 mm-wide annular electron beam.[25] This beam was transported through the SWS using a guiding magnetic field $B = 2.5$ T (axial non-uniformity of $\sim$1% along $\sim$70 cm length), with a half period of $\sim$4.4 ms, produced by an external solenoid.

The cathode, SWS, and solenoid were aligned using specially made adjustment bolts allowing a slight deflection of the SWS structure with respect to the solenoid tube axis and the electron beam pattern obtained by a CR-39 plastic placed at the end of the SWS. This alignment allowed us to obtain the electron beam asymmetry across the SWS of <0.2 mm. The voltage and current waveforms were measured at the vacuum side of the insulator by a capacitive voltage divider and self-integrated Rogowski coil. The electron beam current was measured by a low-inductance and low-resistive Faraday cup (time response $\sim$0.3 ns). In these experiments, the electron beam was transported in a 32 mm inner diameter, 60 cm long stainless steel tube that replaced the SWS, and the Faraday cup was located at the output of this tube. The energy of electrons was determined using the same Faraday cup with Al foils of different thicknesses, placed in front of it. The background pressure ($\sim$6 mPa) in the diode, SWS, mode converter, and horn antenna was maintained by a turbo-molecular pump. The total current of the diode was monitored using a self-integrated Rogowski coil. In the main series of experiments with microwave generation, i.e., with the SWS, this Rogowski coil was removed in order to decrease the inductance of the cathode holder.

The SWS is similar to that described in Ref. 22. It was assembled using 29 ring-type cavities having an inner diameter of 32 mm and outer diameter increasing in the direction of the electron beam propagation, which increases the beam-wave coupling impedance. The increase in the coupling

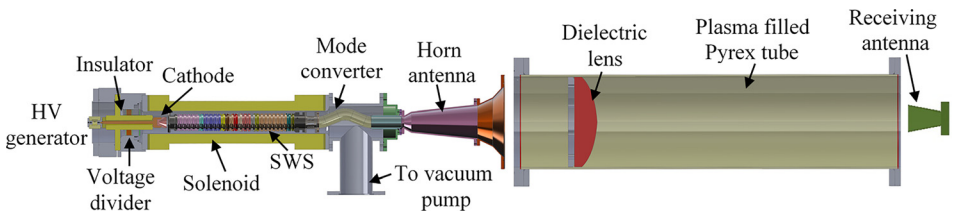

FIG. 1. Experimental system drawing. In the present experiment, the Pyrex tube was not filled with plasma.

impedance allows one to obtain an almost constant electric field in the synchronous harmonic interacting with the beam, despite the growth of the electromagnetic power propagating backward along the SWS.[20] This method increases the efficiency of the conversion of the electron beam kinetic power to the HPM pulse. A low-Q factor cavity for reflection of the wave was placed at the SWS upstream end to provide forward propagation of the generated HPM pulse. A curved waveguide placed at the exit of the SWS, served as a mode converter transforming the TM_{01} mode (operating mode of the BWO) into TE_{11} mode. The latter radiates in the form of a linearly polarized Gaussian beam through a specially designed cylindrical horn antenna. The microwave beam has a width of ~5 cm FWHM of the waist located at ~10 cm upstream the antenna output aperture (the inner surface of the Perspex interface insulator). A photo of the SR-BWO, mode converter, and antenna is presented in Fig. 2.

A hyperbolic dielectric (Ultem, dielectric constant $\varepsilon_r \approx 3$) lens (diameter of 34 cm) was placed at a variable distance with respect to the output of the horn antenna. The experimental results presented in this paper were obtained with this lens. In experiments with the interaction of the HPM and plasma, however, a lens will be inserted inside a Pyrex tube with an inner diameter $\phi = 24$ cm. Thus, for microwave wake-field experiments, two different lenses were designed with a beam waist ρ_0 of 3.6 cm and 6 cm and Rayleigh lengths $z_R = \pi\rho_0^2/\lambda$ of ~14 cm and ~38 cm, respectively (these lenses are described at the beginning of Section IV). Here, a wavelength $\lambda = 3$ cm was considered. The parameters of the inductively coupled plasma, generated in either Ar or He gases in a Pyrex tube by RF (2 MHz) quadruple antenna, were characterized using different electrical, microwave, and spectroscopic diagnostics.[26]

The transmitting properties of the horn antenna were verified using a network analyzer (Anritsu model 54147A). Namely, the output of the analyzer was connected to a standard WR90 coax-to-waveguide adapter, which was connected to a transition adapter from a WR90 rectangular to ϕ28 circular waveguide. Thus, 10 GHz microwaves generated by the analyzer were transmitted through this waveguide in a pure TE_{11} mode and were radiated by the horn antenna. The far-field radiation pattern was studied using a standard WR90 10 dB-gain receiving antenna, both with and without the lens.

The parameters of the high-power microwaves were measured in free space (without the Pyrex tube) using the same receiving antenna placed at different distances with respect to the output of the horn antenna and lens. The receiving antenna was aligned to the center of the transmitting antenna, and the x-y plane was scanned to record the Gaussian beam profile. Similar profile measurements were performed with the dielectric lens, positioned at different distances with respect to the horn antenna output. All the microwave measurements were performed inside a specially built anechoic room (2 m × 1.2 m × 1.8 m) covered by microwave absorbing material (17 dB at 10 GHz). The microwave signal from the receiving antenna and the voltage pulse from the capacitive divider were recorded by a 12 GHz digitizing oscilloscope (Agilent DSO81024B). The power delivered to the receiving antenna was calculated from the registered RF voltage, taking into account the attenuation in the connecting cables and attenuators. The total transmitted power, considering a Gaussian beam, was calculated by integrating the power across the beam at the plane at which the profiles were measured

$$P_t = 2\pi S_0 \int_0^\infty \exp\left(-\frac{2r^2}{\rho^2}\right) r dr = \frac{\pi\rho^2}{2} S_0, \qquad (2)$$

where S_0 is the power flux at the center of the beam, r is the distance from the axis, and ρ is the beam width at the measured plane. The measurements of the microwave power were verified with a calibrated 10 GHz field-free D-dot (Montena SFE10G). The two methods gave similar results, with a difference of <5%. In addition, the microwave beam pattern was obtained by positioning a board with a set of Neon micro-lamps (ϕ5 mm) placed at the distance of ~0.5 m with respect to the horn antenna output.

III. EXPERIMENTAL RESULTS AND DISCUSSION

Typical waveforms of the voltage and electron beam current, and the pattern of the electron beam are shown in Fig. 3. One can see that the beam current has a plateau with a duration of ~2 ns, where the voltage and beam current amplitudes reach ~260 kV and ~1.5 kA, respectively. Here, let us note that in these experiments, the amplitude of the diode total current reached ~2.2 kA. The fact that the amplitude of the diode current is larger than that of the beam current can be related to the backward electron current typical of magnetically insulated diodes. In addition, the rise time and amplitude of the voltage were found to be dependent on the gas (dry air) pressure in the spark gap switch. Namely, by varying the gas pressure in the range 40–70 psi, the voltage amplitude, and rise time are changed in the range from 250–290 kV and 1.5–1 ns, respectively. The obtained beam pattern shows its azimuthal uniformity and that the thickness of the beam is ≤0.6 mm, which corresponds to an electron beam current density of ~1.5 kA/cm^2. The amplitude of the

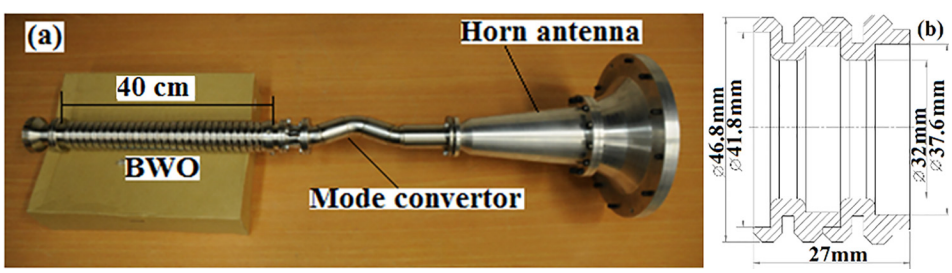

FIG. 2. Appearance of the SR-BWO, mode converter, and horn antenna (a) and zoom of the part of the BWO slow wave structure (b).

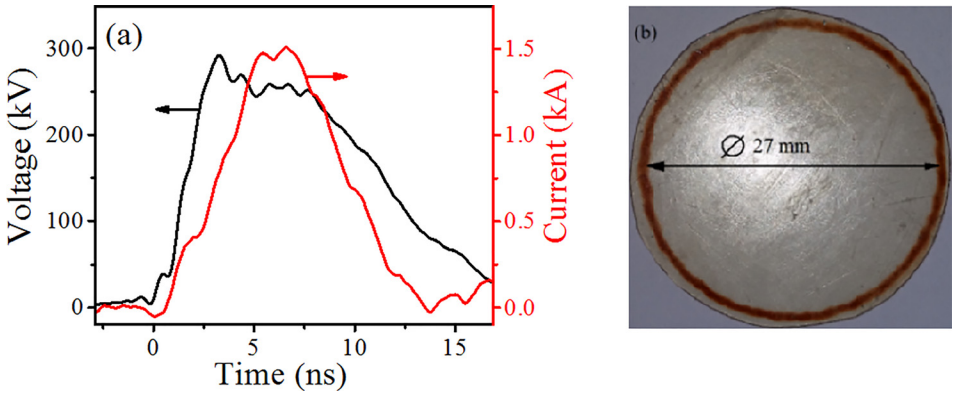

FIG. 3. Typical waveforms of the voltage and electron beam current (a) and the pattern of the electron beam (b). Electron beam current time was shifted, taking into account the propagation time of the electron beam to the Faraday cup.

electron beam current registered by the Faraday cup decreases to ∼200 A after the application of Al foils with a total thickness of 0.22 mm placed in front of it. The latter corresponds to a continuous slowing down approximation range for electrons in the Al target of ∼220 keV.[27] Rough estimates showed that the electrons acquire ∼30 keV in azimuthal and Larmor rotation. Thus, the total kinetic energy of the electrons is ∼250 keV, which agrees satisfactorily with the data obtained by the voltage divider.

The waveform of the microwave electric field, measured at 120 cm from the horn antenna, and the calculated microwave instantaneous and averaged power over a period are shown in Fig. 4. One can see that the maximal electric field amplitude reaches ∼12 kV/cm at that distance and that the total real power of the microwave beam having a duration of ∼0.5 ns, reaches ∼550 MW. This microwave beam power was obtained in shots when the amplitude and rise time of the voltage were ∼290 kV and ∼1 ns, respectively. In shots with a smaller voltage amplitude and a longer rise time, the microwave power was in the range 400–450 MW. The central frequency of the microwaves was found to be 9.6 GHz. The pattern of the microwave beam obtained at a board with a set of Neon micro-lamps (see, Fig. 4(c)) confirms the TE11 mode of the radiation.

Normalized radial profiles of the microwave beam electric field obtained with the network analyzer and BWO, without and with the dielectric lens, are shown in Fig. 5. One can see that without the lens, the FWHM of the beam, radiated from the antenna is ∼70 cm and ∼80 cm for the cases of the network analyzer and BWO microwave beam, respectively. These FWHM values match the known expansion of a Gaussian beam[28]

$$\rho(z)^2 = {\rho_0}^2 + \frac{(z - z_0)^2 \lambda^2}{\pi^2 {\rho_0}^2}, \tag{3}$$

where z is the distance from the horn antenna, and z_0 is the location of the waist. For $z_0 = -10$ cm and $\rho_0 = 3$ cm (parameters of the horn antenna), the expected beam width at $z = 120$ cm is 72 cm FWHM, which satisfactorily matches the experimental results. The application of the dielectric lens results in significant focusing of the beam, namely, its FWHM decreases to 13–16 cm at a distance of 60 cm from the lens.

The axial dependencies of the microwave beam electric field obtained with the network analyzer and generated by the BWO are shown in Fig. 6. Here, one can see a gradual decrease in the amplitude of the electric field along the microwave beam propagation without the lens. This decrease matches the known decrease in amplitude at the center of a Gaussian beam expansion $E(z) = E_0\rho_0/\rho(z)$, for the same parameters, ρ_0 and z_0, described above. Here, E_0 is the field at the center of the beam waist. The application of the lens results in the microwave beam being focused at a distance of ∼40 cm from the lens.

Thus, these experimental results show that the SR-BWO, combined with a mode converter and antenna, radiates a well-defined Gaussian microwave beam with a frequency of

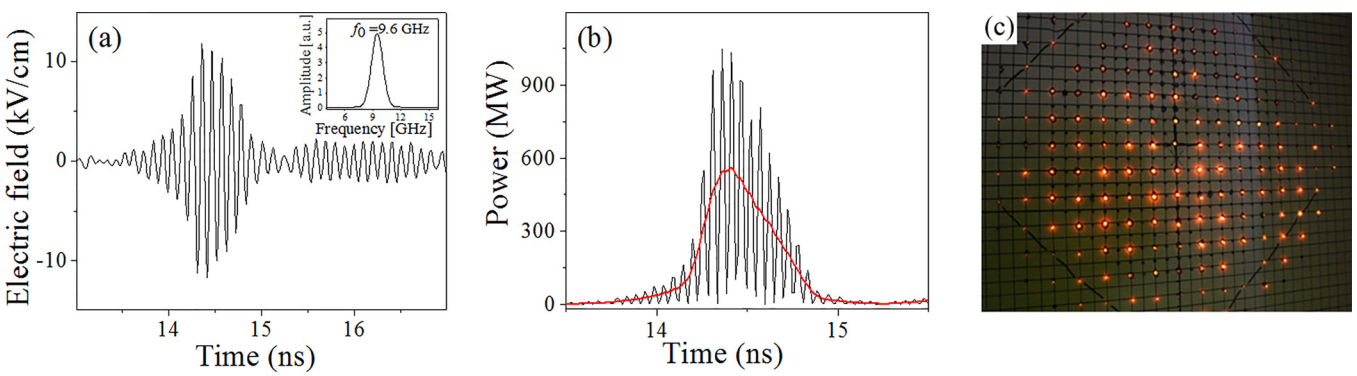

FIG. 4. (a) Waveform of the measured electric field at a distance of 120 cm from the horn antenna; inset: FFT of the microwave signal; (b) calculated total microwave instantaneous power and averaged power over period, where time $t = 0$ is with respect to the beginning of the electron beam current at the output of the BWO; (c) microwave beam pattern obtained at a distance of 0.5 m from the horn antenna.

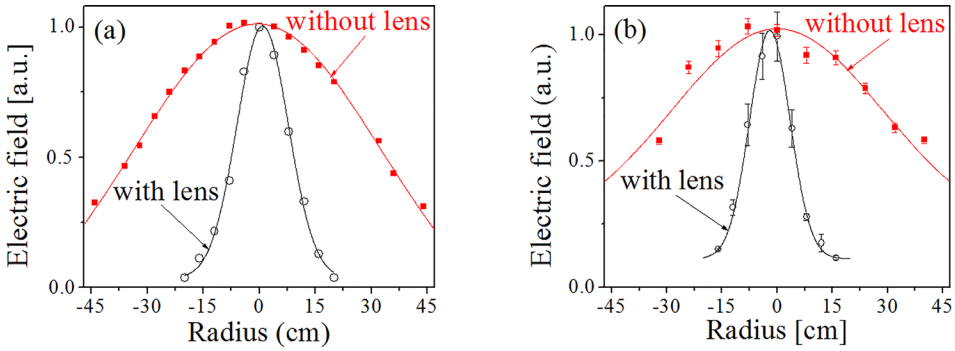

FIG. 5. Radial distributions of the microwave beam normalized electric field obtained with network analyzer (a) and with the BWO (b), without the lens—at a distance of 120 cm from the transmitting antenna, and with the lens, at a distance of 60 cm from the lens. The lens was positioned 20 cm from the transmitting antenna. Solid lines—Gaussian fit.

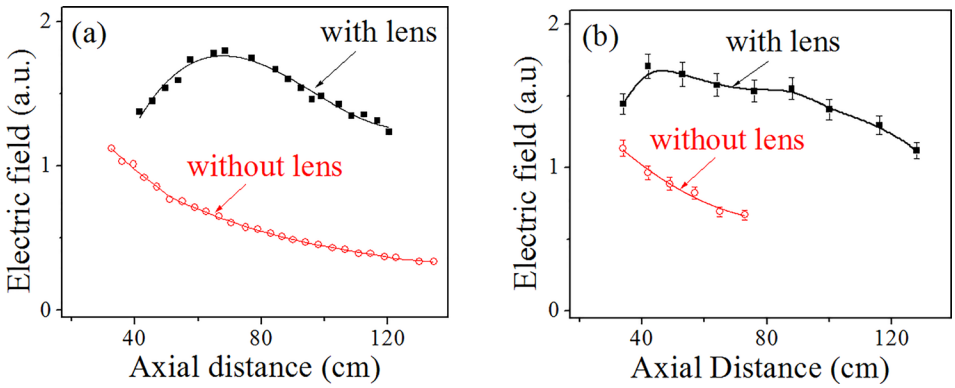

FIG. 6. (a) Profiles of the microwave beam electric field along the axis of the antenna obtained with and without lens: (a) with network analyzer; (b) with BWO. The lens was placed at a distance of ~20 cm from the horn antenna.

9.6 Hz, total power of ~550 MW, and pulse duration of ~0.5 ns, and that the application of the dielectric lens allows one to obtain an electric field up to ~6 MV/m at the focus.

IV. A NUMERICAL FEASIBILITY ANALYSIS OF THE WAKEFIELD EFFECT

Full 3-D simulations of the electron dynamics in the SR-BWO, together with microwave generation and propagation, were performed using the MAGIC electromagnetic particle-in-cell (PIC) code.[29] In this modeling, an electron beam with an amplitude of 1.5 kA emitted from a 0.3 mm thick edged plasma cathode (voltage amplitude of 270 kV and pulse width of 8 ns FWHM) in the presence of a guiding magnetic field of 2.5 T was considered.

The positions of the electrons, the E_r component of the microwave field and the kinetic energy of the electrons along the SWS are shown in Figs. 7(a)–7(c) for time $t = 9.2$ ns with respect to the beginning of the voltage pulse. The oscillating electron's kinetic energy reflects the dynamics of this system; that is, the oscillation grows with the length of the electron beam propagation, efficiently transferring the electron energy to the electromagnetic wave. The total emitted power as a function of time obtained by the simulation is shown in Fig. 7(d). The power in this simulation reaches a peak value of ~450 MW, and the pulse width is 0.5 ns FWHM, which agrees satisfactorily with the obtained experimental results.

The simulation of the microwave propagation after the mode converter was performed by injecting a pure TE_{11} mode into the $\phi 28$ mm circular waveguide, which is connected to the horn antenna. The simulation took into account also the lens and the dielectric window at the exit of the horn antenna. The geometry and results of the simulation are shown in Fig. 8. One can see that, for an input power of 550 MW, the maximal electric field after the focusing is ~7 MV/m. The maximal electric field at the distance of 60 cm from the lens is ~5 MV/m and the width is 13 cm FWHM.

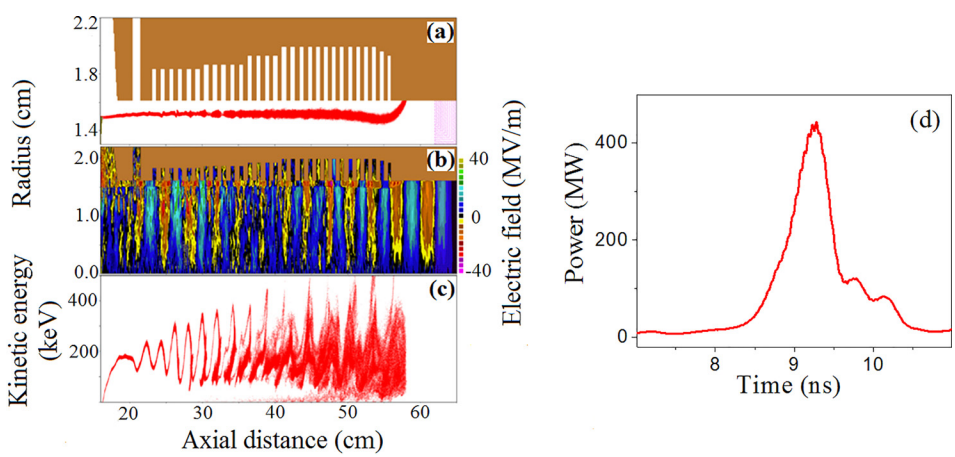

FIG. 7. Results of PIC simulations. Electron positions (a), the radial electric field (b) and the kinetic energy of the electrons (c) along the SWS at time $t = 9.2$ ns with respect to the beginning of the voltage pulse, (d) microwave power at the exit of the BWO. Time $t = 0$ is with respect to the beginning of the voltage pulse.

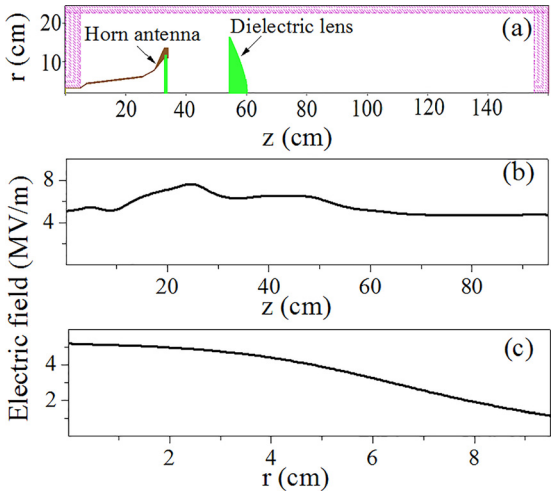

FIG. 8. Simulation geometry of the microwave propagation after the mode converter (a), showing the waveguide, horn antenna, window, and lens. The axial profile of the electric field amplitude with respect to the lens placed at 20 cm from the horn antenna output (b), and the radial profile of the microwave electric field amplitude at a distance of 60 cm from the lens (c).

These results are in good agreement with the experimental results.

The feasibility of wakefield formation in plasma using a high-power microwave beam was tested by numerical simulations. In these simulations, the propagation and focusing of the microwave beam were considered for the geometry of the present experimental setup containing the horn antenna window, lens, Pyrex tube, and dielectric flange with dielectric rods used to support the lens. The lens is located inside the Pyrex tube, in order to allow focusing of the microwave beam inside the plasma chamber. Two lenses with a waist of 6 cm (Rayleigh length of 40 cm) and of 3.8 cm (Rayleigh length of 14 cm) were considered. The simulation results are shown in Fig. 9. One can see that in the case of the long focus lens, the maximum amplitude of the electric field inside the plasma is 10 MV/m and the focus is located at a distance of 20 cm from the lens. In this configuration, the interaction length of the microwave with the plasma will be relatively large, namely, ~40 cm. Stronger focusing can be achieved with the short focus lens when the maximum electric field of 16 MV/m is reached at a distance of 10 cm from the lens. However, in the latter case, the interaction length is much shorter than in the case of the long focus lens.

Preliminary numerical simulations of the microwave-plasma interaction were performed for the short focus lens using the 3D-PIC code Lsp (Large scale plasma),[30] which implement advanced plasma modeling algorithms. The dielectric box (permittivity $\varepsilon_r = 2$) of dimensions 24 cm (x) × 24 cm (y) × 60 cm (z) is filled by the plasma having a uniform electron density of $10^{10}\,\mathrm{cm}^{-3}$. A smaller box of dimensions 6 cm (x) × 6 cm (y) × 15 cm (z) centered at $z = 0$, is filled with electrons and mobile protons producing a quasi-neutral plasma. Outside this box at each electron position, an immobile ion charge is considered. A Gaussian shaped microwave beam with a wavelength of 3 cm and instantaneous maximum power of ~700 MW, cylindrically symmetric with respect to the Z-axis of its propagation, is applied at $z = -10$ cm and focused at $z = 0$ cm where the center of the beam waist is located. The beam "spot-size" at the focal plane was set to 3.8 cm FWHM. The microwave pulse envelope at the horn plane varies in time as $\propto \exp\left[-(t - 1\,\mathrm{ns})^2/0.25\,\mathrm{ns}\right]$, resulting in a beam duration of ~0.8 ns. In Fig. 10, the temporal and spatial dependence of the microwave source is presented. One can see that for $t > 2$ ns, the microwave pulse has almost left the focal region and that the maximum electric field associated with this pulse is ~17 MV/m. When the microwave pulse crosses the focal region, the ponderomotive force is the largest, pushing out the electrons and forming a large positively charged bubble having the size of the order of the microwave beam waist. When the microwave pulse leaves the focal region, the positively charged bubble attracts nearby electrons. This electron "cloud," oscillating around the bubble, forms the localized wakefield, the frequency of which is equal to the electron plasma frequency. In Fig. 11, the simulated results for this localized wake evolution are presented. One can see that the electron charge density oscillates with a period $\tau_w \sim 1$ ns, which is close to the plasma electron frequency $f_p = 1$ GHz. Thus, the focused microwave beam of ~0.7 GW power excites near the focal plane *localized wake*-fields with a strength ~0.5 MV/m. These expected values of electric field and charge density modulation can be directly measured using the temporal- and spatial-dependent diagnostics. This

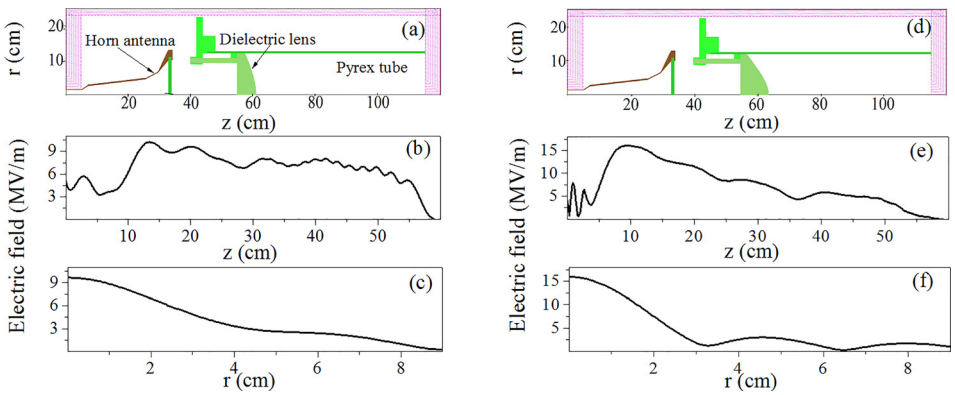

FIG. 9. Simulation geometry of the microwave focusing inside the Pyrex tube with the long (a) and short (d) focus lens showing the waveguide, horn antenna, window, lens, Pyrex tube and dielectric rods; the axial profile of the electric field with respect to the lens placed at 20 cm from the antenna output ((b) and (e)); the radial profile of the electric field at a distance of 20 cm from the long (c) focus lens and at a distance of 10 cm from the short (f) focus lens.

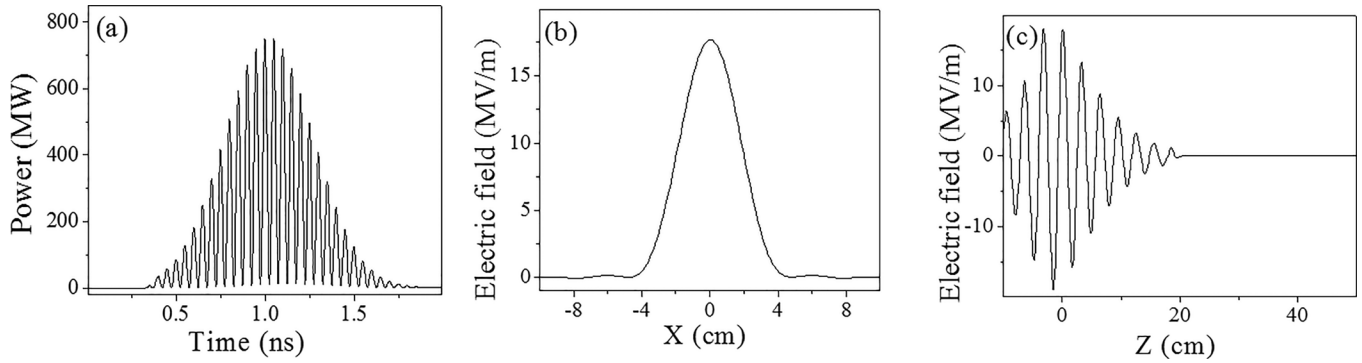

FIG. 10. (a) The instantaneous power of the microwave source at $z = 0$ cm, $x = y = 0$ vs. time. (b) A snapshot of the electric field E_x at $t = 1.0$ ns along the X-axis ($y = z = 0$). (c) A snapshot of the electric field E_x at $t = 1.0$ ns along the Z-axis at $x = y = 0$.

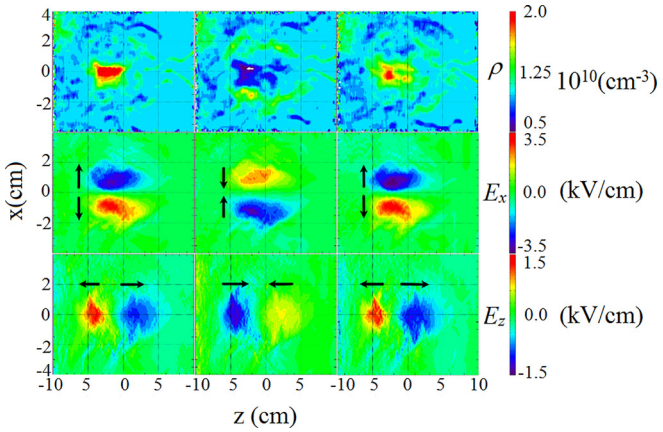

FIG. 11. Electron density, ρ, contours (first row), contours of E_x (second row), and contours of E_z (third row) at $t = 3$ ns (first column), 3.58 ns (second column), and 4.05 ns (third column). For electric field contour plots, the arrows represent the direction of the electron motion resulting from the corresponding electric field.

wake electric field has almost equal longitudinal and transverse components. The latter is different from the wakefield produced by a pulsed laser beam in plasma, because the diameter of the beam is larger than its length, and the wakefield is mainly longitudinal.[2]

The average kinetic energy of the electrons and protons, in a box of dimensions 4 cm $(x) \times 4$ cm $(y) \times 4$ cm (z) centered at $z = 0$, is presented in Fig. 12. The particles' motion

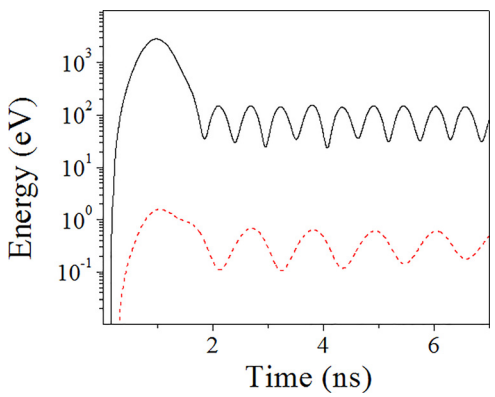

FIG. 12. Average kinetic energy of a plasma electron (full line) and a proton (dashed line) in a box of dimensions 4 cm $(x) \times 4$ cm $(y) \times 4$ cm (z) centered at $Z = 0$.

can be considered for two stages. In the initial stage, where the microwave field is strong at the focus, large energy is acquired by the plasma electrons, and a considerably smaller energy is deposited on the heavier protons. This initial stage ends when the pulse has left at $t > 2$ ns, followed by an oscillatory behavior at much smaller energy levels accompanying the wake. The protons are heated in this process by an average energy of ~0.3 eV, with a modulation that reaches ~0.8 eV. This heating process can lead to Doppler broadening and change in the light intensity of the plasma hydrogen lines, which can be measured in the experiment.

V. CONCLUSIONS

The experimental and numerical studies showed that the application of an SR-BWO powered by a 5 ns-duration high-current electron beam with a peak amplitude of 1.5 kA and electron energy exceeding 200 keV results in the generation of a high-power microwave beam (~550 MW, 0.5 ns, ~9.6 GHz). The focusing of this microwave beam by dielectric lens should be suitable for wake-field generation in under-dense plasma producing a density modulation of almost 100%, and longitudinal and transverse electric field of a few kV/cm in a localized wake. It is understood that the expected wakefield will be several orders lower than those obtained as a result of powerful and ultrashort laser beam interaction with dense plasma (with, e.g., $\sim 10^{11}$ V/m field strength, $\sim 10^{19}$ W/cm^2 power density, 10^{-13} s pulse duration, and $\sim 10^{18}$ cm^{-3} electron density). However, this method allows the application of different time- and space-resolved diagnostics for characterization of the plasma parameters which determine the formation and evolution of the wakefield and comparison between experimental and simulations results. In addition, taking into account a fast progress in the generation of short duration microwave pulses with a power of several GW,[31] one can consider this method for charged particles acceleration to moderate energies[16] as well.

ACKNOWLEDGMENTS

The authors are grateful to A. Fisher for fruitful discussions, to E. Flyatt for technical assistance, and to Dale Welch and Chris Mostrom of Voss Scientific, Inc., for their assistance in setting up and running Lsp. This work was

supported in part by the PAZY Grant No. 2020960 and by the Center for Absorption in Science, Ministry of Immigrant Absorption, State of Israel.

[1]T. Tajima and J. Dawson, Phys. Rev. Lett. **43**, 267 (1979).
[2]E. Esarey, C. Schroeder, and W. Leemans, Rev. Mod. Phys. **81**, 1229 (2009).
[3]V. Malka, Phys. Plasmas **19**, 55501 (2012).
[4]W. P. Leemans, B. Nagler, A. J. Gonsalves, C. Tóth, K. Nakamura, C. G. R. Geddes, E. Esarey, C. B. Schroeder, and S. M. Hooker, Nat. Phys. **2**, 696 (2006).
[5]S. P. D. Mangles, C. D. Murphy, Z. Najmudin, A. G. R. Thomas, J. L. Collier, A. E. Dangor, E. J. Divall, P. S. Foster, J. G. Gallacher, C. J. Hooker, D. A. Jaroszynski, A. J. Langley, W. B. Mori, P. A. Norreys, F. S. Tsung, R. Viskup, B. R. Walton, and K. Krushelnick, Nature **431**, 535 (2004).
[6]M. Litos, E. Adli, W. An, C. I. Clarke, C. E. Clayton, S. Corde, J. P. Delahaye, R. J. England, S. Fisher, J. Frederico, S. Gessner, S. Z. Green, M. J. Hogan, C. Joshi, W. Lu, K. Marsh, W. B. Mori, P. Muggli, D. Walz, G. White, Z. Wu, V. Yakimenko, and G. Yocky, Nature **515**, 92 (2014).
[7]N. H. Matlis, S. Reed, S. S. Bulanov, V. Chvykov, G. Kalintchenko, T. Matsuoka, P. Rousseau, V. Yanovsky, A. Maksimchuk, S. Kalmykov, G. Shvets, and M. C. Downer, Nat. Phys. **2**, 749 (2006).
[8]M. B. Schwab, A. Sävert, O. Jäckel, J. Polz, M. Schnell, T. Rinck, L. Veisz, M. Möller, P. Hansinger, G. G. Paulus, and M. C. Kaluza, Appl. Phys. Lett. **103**, 191118 (2013).
[9]P. Gibbon, *Short Pulse Laser Interactions with Matter* (World Scientific Publishing, 2005).
[10]Y. Nishida, S. Kusaka, and N. Yugami, Phys. Scr. **1994**, T52 (1994).
[11]H. Ito, Y. Nishida, and N. Yugami, Phys. Rev. Lett. **76**, 4540 (1996).
[12]M. Kamal-Al-Hassan, H. Ito, N. Yugami, and Y. Nishida, Phys. Plasmas **12**, 112307 (2005).
[13]H. Ito, C. Rajyaguru, N. Yugami, Y. Nishida, and T. Hosoya, Phys. Rev. E **69**, 066406 (2004).
[14]G. M. Batanov, V. A. Ivanov, M. E. Konyzhev, A. A. Ravaev, V. D. Selesnev, and A. I. Khomenko, in *Proceedings of the International Workshop on "Strong Microwaves in Plasmas"* (1991), Vol. 2, p. 553.
[15]A. K. Aria and H. K. Malik, Open Plasma Phys. J. **1**, 1 (2008).
[16]H. K. Malik and S. Kumar, Laser Part. Beams **26**, 197 (2008).
[17]A. K. Aria and H. K. Malik, Opt. Commun. **282**, 423 (2009).
[18]J. Benford, J. Swegle, and E. Schamiloglu, *High Power Microwaves*, 3rd ed. (CRC Press, Taylor & Francis Group, Boca Raton, London, New York, 2016).
[19]N. S. Ginzburg, N. Y. Novozhilova, I. V. Zotova, A. S. Sergeev, N. Y. Peskov, A. D. Phelps, S. M. Wiggins, A. W. Cross, K. Ronald, W. He, V. G. Shpak, M. I. Yalandin, S. A. Shunailov, M. R. Ulmaskulov, and V. P. Tarakanov, Phys. Rev. E: Stat. Phys., Plasmas, Fluids, Relat. Interdiscip. Top. **60**, 3297 (1999).
[20]A. A. Eltchaninov, S. D. Korovin, V. V. Rostov, I. V. Pegel, G. A. Mesyats, S. N. Rukin, V. G. Shpak, M. I. Yaladin, and N. S. Ginzburg, Laser Part. Beams **21**, 187 (2003).
[21]N. S. Ginzburg, I. V. Zotova, A. W. Cross, A. D. R. Phelps, M. I. Yalandin, and V. V. Rostov, IEEE Trans. Plasma Sci. **41**, 646 (2013).
[22]A. A. El'chaninov, S. D. Korovin, V. V. Rostov, I. V. Pegel, G. A. Mesyats, M. I. Yalandin, and N. S. Ginzburg, JETP Lett. **77**(6), 266 (2003).
[23]N. S. Ginzburg, I. V. Zotova, I. V. Pegel, V. V. Rostov, V. G. Shpak, and M. I. Yalandin, Radiophys. Quantum Electron. **50**, 762 (2007).
[24]S. N. Rukin, Instrum. Exp. Tech. **4**, 439 (1999).
[25]G. Shafir, M. Kreif, J. Z. Gleizer, S. Gleizer, Y. E. Krasik, A. V. Gunin, O. P. Kutenkov, I. V. Pegel, and V. V. Rostov, J. Appl. Phys. **118**, 193302 (2015).
[26]G. Shafir, D. Zolotukhin, V. Godyak, A. Shlapakovski, S. Gleizer, Ya. Slutsker, R. Gad, V. Bernshtam, Yu. Ralchenko, and Ya. E. Krasik, "Characterization of inductively coupled plasma generated by a quadruple antenna," Plasma Sources Sci. Technol. (to be published).
[27]M. J. Berger, J. S. Coursey, M. A. Zucker, and J. Chang, see http://www.nist.gov/pml/data/star/index.cfm for NIST (2011).
[28]L. V. Tarasov, *Laser Physics* (MIR Publishers, Moscow, 1983).
[29]B. Goplen, L. Ludeking, D. Smith, and G. Warren, Comput. Phys. Commun. **87**, 54 (1995).
[30]Orbital ATK, Inc., see http://www.mrcwdc.com/LSP/index.html for "Particle-in-Cell (PIC) code for Large Scale Plasma Simulations."
[31]V. V. Rostov, I. V. Romanchenko, M. S. Pedos, and M. I. Yalandin, Phys. Plasmas **23**, 093103 (2016).